Zeolitic Imidazolate Frameworks Hot Paper

How to cite:
International Edition: doi.org/10.1002/anie.202207467
German Edition: doi.org/10.1002/ange.202207467

Zeolite NPO-Type Azolate Frameworks

Xiangyi Zha[+], Xinhao Li[+], Abdulhadi A. Al-Omari[+], Shan Liu, Cong-Cong Liang, Ala'a Al-Ghourani, Mahmoud Abdellatief, Jingjing Yang, Ha L. Nguyen, Bassem Al-Maythalony, Zhaolin Shi,* Kyle E. Cordova,* and Yue-Biao Zhang**

Abstract: Three-membered rings (3-rings) are an important structural motif in zeolite chemistry, but their formation remains serendipitous in reticular chemistry when designing zeolitic imidazolate frameworks (ZIFs). Herein, we report a design principle for constructing four new ZIFs, termed ZIF-1001 to -1004, from tetrahedral Zn^{II} centers (T), benzotriazolate (bTZ), and different functionalized benzimidazolates (RbIM) that adopt a new zeolite NPO-type topology built from 3-rings. Two factors were critical for this discovery: i) incorporating the bTZ linker within the structures formed 3-rings due to a ∠(T–bTZ–T) angle of 120–130° reminiscent of the ∠(Ge–O–Ge) angle (130°) observed in germanate zeolite-type structures having 3-rings; and ii) RbIM guided the coordination chemistry of bTZ to bind preferentially in an imidazolate-type mode. This series' ability to selectively capture CO_2 from high-humidity flue gas and trap ethane from tail gas during shale gas extraction was demonstrated.

Introduction

Zeolitic imidazolate frameworks (ZIFs) are metal–organic analogues to inorganic zeolite-type materials.[1] To date, the design of ZIFs has been limited to three working principles: i) tetrahedral metal centers (T) are bridged by azolate linkers (e.g., imidazolate, IM) to form T–IM–T angles (Figure 1a, 135–145°) that are similar to those Si–O–Si angles (≈145°) observed in pure silica zeolites;[2] ii) linker–linker interactions[3] are used to orient the synthesis without the use of supplementary structure-directing agents;[4] and iii) mixed-linker systems exploit differences in the steric index and ratio of the mixed linkers to achieve ZIFs with extra-large pore apertures and colossal cages.[5] Although these principles have successfully yielded hundreds of unique ZIF structures, a handle over the rational design and targeting of specific end structures often remains elusive.[1,6]

Herein, we propose a synthetic strategy for targeting zeolite azolate frameworks based on three-membered rings (3-rings, Figure 1b). Specifically, we report the design, synthesis, and characterization of an isoreticular series of ZIFs with a new topology of the zeolite NPO net,[6,7] termed ZIF-1001 to -1004, constructed by linking tetrahedral Zn^{II} centers (T) with benzotriazolate (bTZ) linker and benzimidazolate (bIM), 5-methylbenzimidazolate (mbIM), 5-bromobenzimidazolate (bbIM), or 5-chlorobenzimidazolate (cbIM), respectively. Single-crystal X-ray diffraction (SCXRD) confirmed the co-existence of bTZ and bIM within the 3-rings in 2:1 or 1:2 ratios (Figure 1b), which can be distinguished by the T–bTZ–T angles of 122° and the T–bIM–T angles of 133°. Given the nature of the linkers incorporated within this series, we further validate the thermal stability by variable-temperature synchrotron powder X-ray diffraction (PXRD) and the chemical stabilities by PXRD analyses after immersing in boiling water and in aqueous acid/base solutions (pH = 3–14). Owing to their ultramicroporosity, intrinsic hydrophobicity, and chemical stability, these ZIFs performed efficient CO_2 capture from CO_2/N_2 mixtures with high humidity and in simulated flue gas in the presence of SO_x and NO_x, as well as selectively trapping of C_2H_6 from CO_2, which is an important separation process desired for sustainable resource recycling from tail gas during shale gas extraction.

We note that the 3-ring has been a critical structural motif for designing zeolite-type materials.[8,9] In zeolite chemistry, the historical challenge for realizing new struc-

[*] X. Zha,[+] X. Li,[+] S. Liu, Dr. C.-C. Liang, Dr. Z. Shi, Prof. Dr. Y.-B. Zhang
Shanghai Key Laboratory of High-Resolution Electron Microscopy, School of Physical Science and Technology
ShanghaiTech University, Shanghai 201210 (China)
E-mail: shizhl1@shanghaitech.edu.cn
zhangyb@shanghaitech.edu.cn

A. A. Al-Omari[+]
Center of Research Excellence in Nanotechnology (CENT), Department of Chemical Engineering, King Fahd University of Petroleum and Minerals, Dhahran 34464 (Saudi Arabia)

A.'a Al-Ghourani, Prof. Dr. B. Al-Maythalony, K. E. Cordova
Materials Discovery Research Unit, Advanced Research Center, Royal Scientific Society, Amman 11941 (Jordan)
E-mail: bassem.maythalony@rss.jo
kyle.cordova@rss.jo

Dr. M. Abdellatief
Synchrotron-light for Experimental Science and Applications in the Middle East (SESAME), Allan 19252 (Jordan)

Dr. J. Yang, Dr. H. L. Nguyen
Department of Chemistry and Berkeley Global Science Institute, University of California, Berkeley, Berkeley, CA 94720 (USA)

Prof. Dr. B. Al-Maythalony
KACST-TIC on CCS, King Fahd University of Petroleum and Minerals, Dhahran 34464 (Saudi Arabia)

[+] These authors contributed equally to this work.

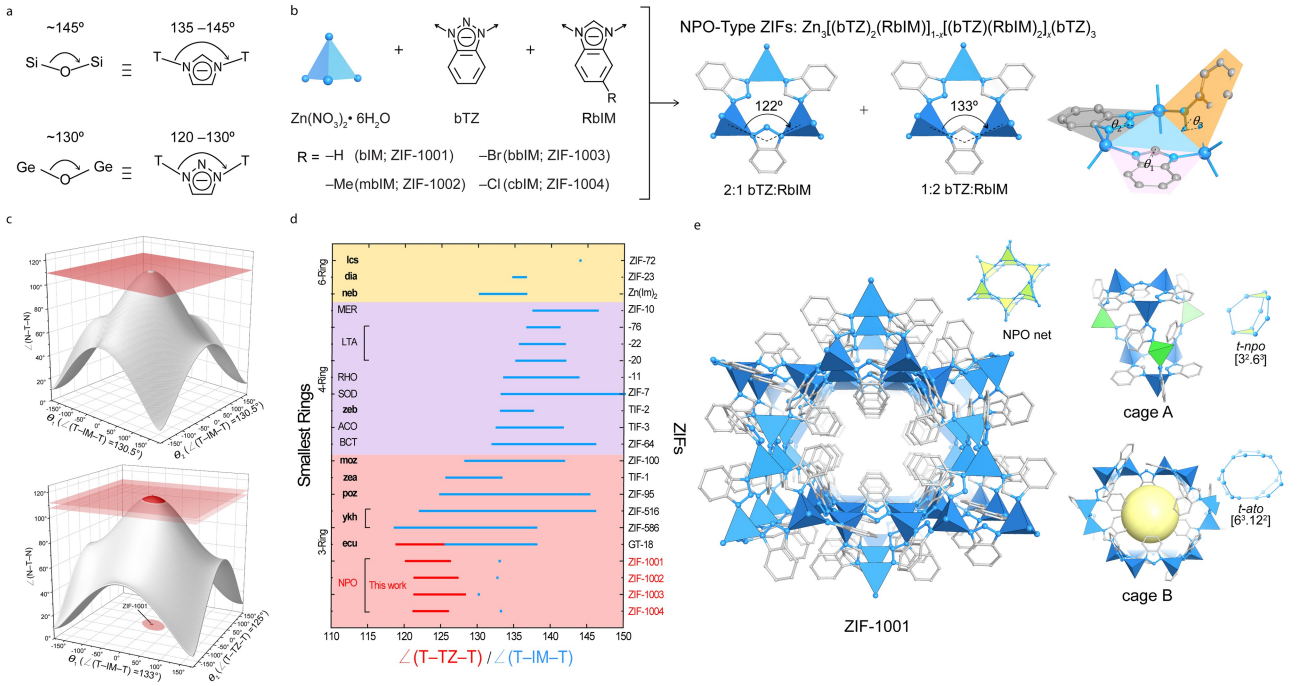

Figure 1. Design principles for targeting zeolite NPO-type azolate frameworks comprised of 3-rings. a) The design of ZIFs is historically based on mimicking the ∠(Si–O–Si) angles of ≈145° in zeolite-type materials through creating ∠(T–IM–T) angles of 135–145°. The design strategy of NPO-type azolate frameworks seeks to create ∠(T–bTZ–T) angles of 120–130° that resemble the ∠(Ge–O–Ge) angles of ≈130° observed in germanate zeolites to lessen the 3-ring strain.[2,8–10] b) Reaction of tetrahedral Zn^{II} and bTZ with different functionalized benzimidazolates (RbIM) yields ZIF-1001 to -1004 comprised of two types of 3-rings with the bTZ and RbIM in different ratios and varying angles, θ_1, θ_2, and θ_3, that deviate away from the 3-ring plane. c) Geometry analysis of the T site for two adjacent linkers via θ_1 and θ_2 angles when the ∠(T–IM–T) angle for the adjacent linkers are both 130.5° (top) and when the ∠(T–TZ–T) angle is 125° and the ∠(T–IM–T) angle is 133° (bottom). d) The ∠(T–IM–T) angle distribution of IM linkers in most reported ZIFs ranges from ca. 132–150° meaning that it is difficult find IM linkers that adopt small angles necessary for constructing 3-rings with low ring strain. A ∠(T–TZ–T) angle of <130° (highlighted in red) reported herein leads to the formation of the NPO net, which is nearly impossible for ∠(T–IM–T) angles centered at 135–145°. e) Crystal structure of ZIF-1001 adopts a distorted NPO-type net featuring 1D channels that proliferate along the *a*-axis. Cage A (*t-npo*, $[3^2.6^3]$) is built from two parallel 3-ring units that are connected by three bTZ–Zn–bTZ bridges. Cage B (*t-ato*, $[6^3.12^2]$) is constructed from six cage A units that form a 12-ring opening. All insets depict the underlying net of the corresponding crystal structures. The embedded natural tiling is noted in face symbol, [..m^n..], meaning that there are *n* faces with *m*-membered rings. The yellow ball is a visual representation of the free space available in the pore. Atom colors: Zn, blue and green polyhedra; C, gray; N, blue. All H atoms are omitted for clarity.

tures based on 3-rings is a need to compensate for the large strain of inorganic rings, which can be accomplished by varying the T centers away from Si to elements with larger atomic radii, such as Ge, in order to increase the T–O bond length and decrease the ∠(T–O–T) angle (Figure 1a).[9] Although ZIF structures containing 3-rings have been reported (e.g., ZIF-95 and ZIF-100 with the **poz** and **moz** nets, respectively, TIF-1 with the **zea** net, GT-18 with the **ecu** net, and ZIF-516/586 with **ykh** net), the chemical realization of their design principles remains severely underdeveloped.[10–12,5c] The critical discovery in this series is therefore two-fold: i) incorporating a large amount of bTZ within the structures enabled the formation of 3-rings due to a ∠(T–bTZ–T) angle of 120–135°, being achieved, which is reminiscent of the ∠(Ge–O–Ge) angle (≈130°) observed in zeolite-type germanate structures based on 3-rings. Indeed, the reduction of the ∠(T–bTZ–T) angle relieves the ring strain in 3-rings, and ii) bIM guided the chemistry of bTZ to bind preferentially in the imidazolate-type mode. This new design principle reduced ∠(T–bTZ–T) angles when compared to previously reported ZIF structures, which led to the formation of ideal tetrahedral centers and 3-ring motifs (Figure 1c,d).

Results and Discussion

Constructing ZIFs based on 3-rings from the traditional ∠(T–IM–T) angle of 135–145° is challenging when considering the geometry of an ideal T center requiring a ∠(IM–T–IM) angle of 109.5°. Forming co-planar 4- to 10-rings in ZIFs that have an ideal T center is possible when the ∠(T–IM–T) angle is 144°. This ∠(T–IM–T) angle is achieved by flipping two adjacent T–IM bonds in a plane resulting in a ∠(T_1–T_2–T_3) angle of 73.5–145.5°, which excludes the possibility of forming a 3-ring.[4b] In targeting 3-rings, we coded a geometric model for free rotation of adjacent T–IM bonds that have angles, θ_1 and θ_2, away from the plane of a given ring. The corresponding ∠(IM–T–IM) angle with the ∠(T–IM–T) angle being fixed can then be calculated. Consequentially, we then can evaluate the possibility of forming 3-rings for a certain ∠(T–IM–T) angle that satisfies

the geometry of an ideal T center with a ∠(IM–T–IM) angle of 109.5 ± 1°. By setting the ∠(T–IM–T) angle to 140°, no appropriate θ_1 and θ_2 angles will yield a 3-ring with an ideal T site. However, by setting ∠(T–IM–T) = 130.5°, θ_1 and θ_2 angles are close to 0° and satisfy the geometry of an ideal T center. It was through this gained understanding of the required ∠(T–IM–T) angles that we were able to develop a synthetic design strategy for realizing a new ZIF structure comprised of 3-rings.

ZIF-1001 to -1004 were synthesized solvothermally using a mixture of $Zn(NO_3)_2 \cdot 6H_2O$, bTZ, and the respective RbIM derivative in *N,N*-dimethylformamide (DMF) at 120 °C for 3 days (Section S1 in the Supporting Information). It is important to point out the roles that both bTZ and bIM and their derivatives play in realizing ZIF-1001 to -1004 under these synthetic conditions. These ZIFs are achievable when synthetic input mole ratios of bTZ:bIM are greater than 1.5:1. At synthetic input mole ratios of bTZ:bIM are less than 1.5:1, the SOD-type ZIF-7 structure is observed. Furthermore, if the bIM derivative is replaced with the less bulky, pure IM linker, then a two-dimensional ZIF is realized with little to no attractive features. Upon completion of the reactions for ZIF-1001 to -1004, needle-like crystals suitable for single-crystal X-ray diffraction analysis were isolated after decanting the mother liquid and washing the crystals with fresh DMF to remove any unreacted starting materials.

All members of the series crystallized in the orthorhombic $P2_12_12_1$ (No. 19) space group (Tables S1–S4 in the Supporting Information).[13] Taking the asymmetric unit of ZIF-1001 as a representative example, the evolution of the 3-ring unit is clearly seen by three tetrahedral Zn^{II} centers being brought together via two bTZ and one bIM linkers or one bTZ and two bIM linkers (Figure 1b, e). This 3-ring unit is then extended further to other 3-ring units through six bTZ linkers that ultimately form a distorted zeolite NPO net having one-dimensional channels proliferating along the *a*-axis [Figure 1e; note: an ideal NPO-type net crystallizes in the space group $P6_3/mmc$ (No. 194)]. The overall distorted NPO net characteristic of this series is defined by two distinct cages (the embedded natural tiling are noted in face symbol [..m^n..]: *n* faces with *m*-membered rings):[14] i) a smaller cage A (*t-npo*, [$3^2.6^3$]) created by two parallel 3-ring units that are connected by three bTZ–Zn–bTZ bridges with dihedral angles of 45.5 or 47.7°; and ii) a larger cage B (*t-ato*, [$6^3.12^2$]) that is derived from six cages A units coming together to form a 12-ring opening to the one-dimensional channel (Figure 1e). The ∠(Zn–bTZ–Zn) angle is ≈122° and the ∠(Zn–bIM–Zn) angle is ≈133°. These values are smaller than the typical ∠(T–IM–T) angles (135–145°) observed in ZIFs, which serve the purpose of reducing the strain of the 3-rings that form the basis for these structures. The framework density (FD; the number of T sites per 1000 Å^3) of ZIF-1001 is 2.75 T nm^{-1}, which is comparable to those ZIFs whose structures adopt zeolite-type nets (e.g., BCT, GIS, and ACO).[2,11]

Prior to further structural characterization, all members of this series were washed with fresh DMF (6 × 10 mL), solvent exchanged with CH_3OH (6 × 10 mL each day for 5 days) and evacuated for 12 h at 120 °C to yield activated samples. The structural stability upon activation and the bulk phase purity of the series was demonstrated by powder X-ray diffraction (PXRD) analysis, in which the experimental diffraction patterns obtained for the activated samples were observed to be in satisfactory agreement with the patterns simulated from the single-crystal structures (Figure 2a). Thermal gravimetric analysis (TGA) indicated that all members of this series had high thermal stability (≈500 °C) and that the activated samples were free of any guest molecules residing within their pores (Figure S11 and Table S6 in the Supporting Information). Temperature-dependent synchrotron PXRD measurements provided absolute confirmation of the high thermal stability for ZIF-1001 up to 500 °C and demonstrated that no structural transformations occurred (Figure 2b). Finally, the examination of the chemical stability for all members of this series was undertaken by immersing activated samples in boiling water for 5 days in addition to aqueous acid/base solutions ranging from pH = 3 to 14 for at least 7 days. Interestingly, all members retained their structures as evidenced by the coincidence of the PXRD patterns with those simulated from the single crystal structure (Figures 2c,d; Figures S15—S19 in the Supporting Information).

The chemical formula for each member of this series was calculated through a combination of digested-solution ^{1}H nuclear magnetic resonance (NMR) spectroscopy, elemental analysis (EA), and metal-oxide residue analysis via TGA under airflow. The relative ratios of the bTZ and bIM linkers incorporated into each of the ZIF structures were first assessed through ^{1}H-NMR spectroscopy (Section S3 in the Supporting Information). For these measurements, activated samples were dissolved in a solution containing DMSO-d_6 and 20 % DCl in D_2O and the ^{1}H signals for each of the linkers were assigned according to characteristic chemical shifts. For all members of the series, a bTZ:bIM linker ratio was established at 3:1, which is consistent with what is observed in their corresponding crystal structures. Given this information, EA data (e.g., for ZIF-1001: calcd, C, 49.9, H, 2.85, and N, 25.6 %; found, C, 48.8, H, 2.39, and N, 24.8 %) was used to support a general chemical formula of $Zn_3[(bTZ)_2(RbIM)]_{1-x}[(bTZ)(RbIM)_2]_x(bTZ)_3$ (where RbIM = bIM, mbIM, bbIM, and cbIM for ZIF-1001 to -1004, respectively) (Section S1 in the Supporting Information). Finally, the calculated ZnO residues (22 %) found in the TGA curves for all members of the series agreed with the value derived from the EA data (23 %) (Table S6 in the Supporting Information).

The permanent porosity of the series was first probed by Ar isotherms at 87 K (Section S6 in the Supporting Information). ZIF-1001 exhibited a typical Type-I profile, which is characteristic of a microporous material, and a Brunauer–Emmett–Teller (BET) surface area of 290 m^2 g^{-1} was calculated. Surprisingly, the other members of the series displayed no appreciable Ar uptake at 87 K, likely due to the limited size of their pore apertures. Reversible CO_2 adsorption was observed for all members at 195 K (Figure 2e). For ZIF-1001, pore size distributions derived using Monte Carlo simulations for the CO_2 isotherm at 273 K

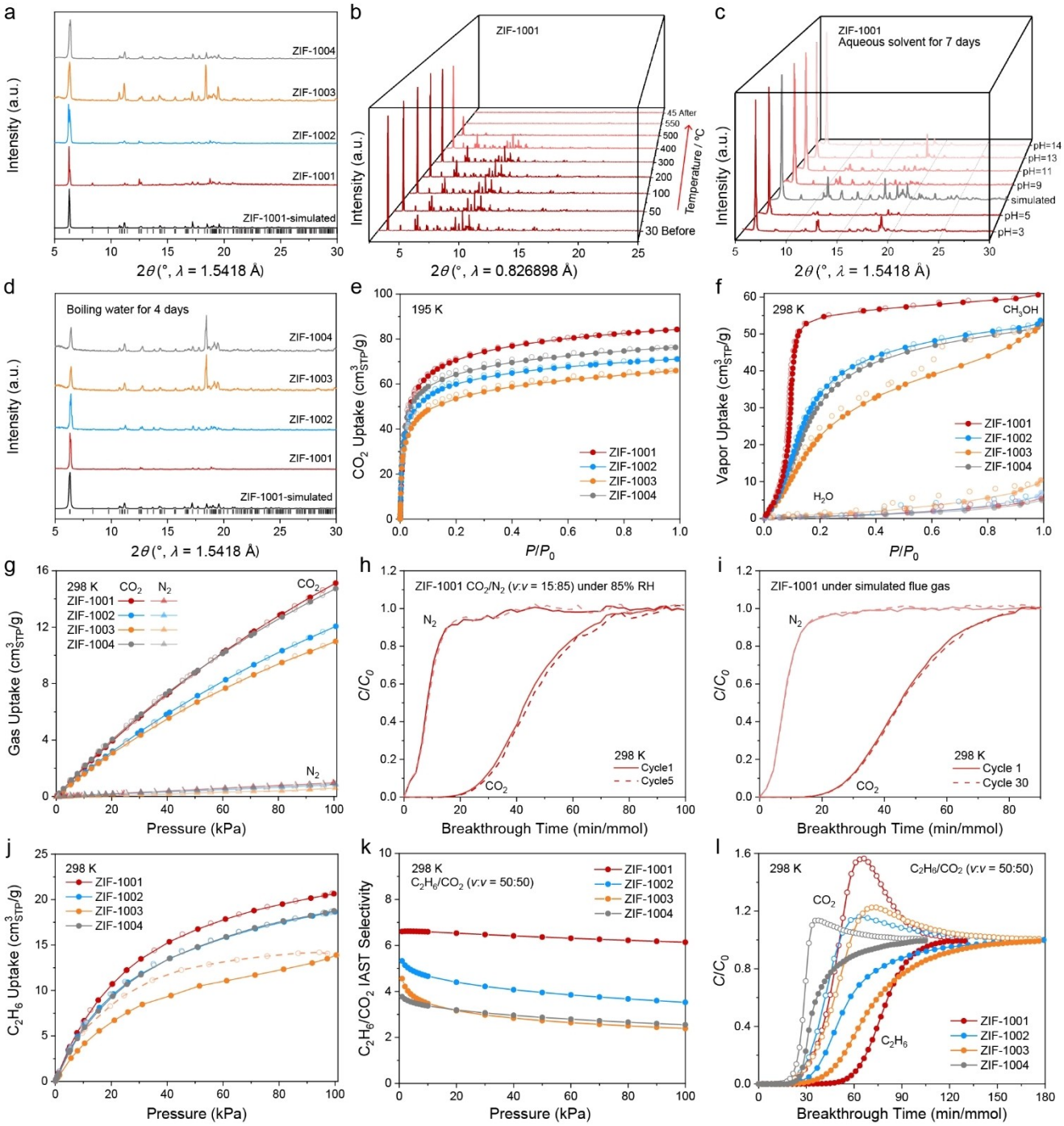

Figure 2. Characterization of the thermal/chemical stability, intrinsic hydrophobicity, ultramicroporosity, and evaluation of the gas sorption and separation properties in NPO-type ZIFs. a) PXRD patterns of the activated ZIF-1001 (red), -1002 (blue), -1003 (orange) and -1004 (grey) compared with the Bragg reflections for the PXRD pattern simulated from the single crystal data (black). b) Temperature-dependent synchrotron PXRD patterns confirm the high thermal stability (500 °C) of ZIF-1001. c) PXRD patterns of ZIF-1001 after immersing in aqueous solutions ranging from pH = 3 to 14 for 7 d. d) PXRD patterns of ZIF-1001 to -1004 after immersing in boiling water for 5 d. e) CO_2 adsorption isotherms at 195 K for ZIF-1001 to -1004 proving this series' ultramicroporosity. f) Methanol and water vapor adsorption isotherms at room temperature for ZIF-1001 to -1004. g) CO_2 and N_2 uptake for ZIF-1001 to 1004 at 298 K. Open and closed symbols represent adsorption and desorption branches, respectively. The connecting line is a guide for the eye. h) Cycling breakthrough curves under high-humidity conditions (85% RH) for the CO_2/N_2 ($v/v = 15:85$) gas mixture at 298 K and a flow rate of 1.0 mL min^{-1}. Solid and dashed lines represent cycles 1 and 5, respectively. i) Cycling breakthrough curves under simulated flue gas conditions (80% N_2, 15% CO_2, 5% O_2, 85% RH, 1000 ppm of SO_2, 500 ppm of NO_2, 298 K and a flow rate of 1.0 mL min^{-1}). Solid and dashed lines represent cycles 1 and 30, respectively. j) C_2H_6 adsorption isotherms at 298 K for ZIF-1001 to -1004. Open and closed symbols represent adsorption and desorption branches, respectively. The connecting line is a guide for the eye. k) C_2H_6/CO_2 IAST selectivity for the C_2H_6/CO_2 ($v/v = 50:50$) gas mixture at 298 K. l) Breakthrough curves for ZIF-1001 to -1004 for a C_2H_6/CO_2 ($v/v = 50:50$) gas mixture at 298 K and a flow rate of 1.0 mL min^{-1}.

(centered at 6.1 Å) and density functional theory models fitted to the Ar isotherm at 87 K (5.7 Å) were in satisfactory agreement (Section S6 in the Supporting Information). Pore volumes (0.150, 0.127, 0.118, and 0.136 $cm^3 g^{-1}$ for ZIF-1001 to ZIF-1004, respectively) were calculated from the CO_2 sorption isotherms at 195 K, which are consistent with the theoretical values obtained from PLATON (0.156, 0.126, 0.113, and 0.132 $cm^3 g^{-1}$, respectively). Finally, water vapor adsorption isotherms were collected for all ZIF members at 298 K using the static volumetric method (Figure 2f). All ZIF members displayed Type III profiles indicating the prominent role that the hydrophobic functionalities distributed throughout the frameworks play.

Given this series' high thermal and chemical stability and hydrophobicity, we sought to assess their effectiveness in the industrially relevant capture of CO_2 from flue gas with high humidity conditions and in the presence of SO_x and NO_x.[15,16] Thermodynamic CO_2 and N_2 adsorption isotherms were subsequently measured at 273, 283, and 298 K (Section S6 in the Supporting Information). At all temperatures and for all members of the series, the adsorption-desorption processes were observed to be completely reversible, and there was noticeably higher uptake and affinity for CO_2 over N_2. The CO_2 uptake capacities at 298 K and 15 kPa (i.e., partial pressure of CO_2 in coal-fired post-combustion flue gas streams) were 3.0, 2.5, 2.4, and 3.2 $cm^3 g^{-1}$ for ZIF-1001 to -1004, respectively (Figure 2g). Coverage-dependent enthalpies of adsorption (Q_{st}) were then calculated by fitting the isotherm data at 273, 283, and 298 K with a virial-type expansion equation (Section S7 in the Supporting Information). The resulting Q_{st} values at zero coverage were $\approx$25–30 $kJ mol^{-1}$—moderate values that indicate a physisorption-driven process. Based on ideal adsorbed solution theory (IAST), by fitting CO_2 and N_2 adsorption isotherms at 298 K and 0–101 kPa, the CO_2/N_2 ($v/v = 15:85$) selectivity was calculated for ZIF-1001 to -1004 (Section S8 in the Supporting Information). At low pressures, ZIF-1003 and ZIF-1004 with halogen functional groups exhibit higher CO_2/N_2 selectivities of 22 and 24, respectively.

To demonstrate the series' proficiency in capturing CO_2 under practical conditions, dynamic gas adsorption breakthrough experiments were carried out using CO_2/N_2 gas mixtures ($v/v = 15:85$ at 298 K and 1.0 bar) under either dry or high-humidity conditions (85 % RH) with a gas mixture flow rate of 1.0 $mL min^{-1}$ (Figure 2h and Section S9 in the Supporting Information). The CO_2 breakthrough time (i.e., the time it takes for CO_2 to "breakthrough" the bed) and kinetics were similar for all members under both dry and high-humidity conditions. This is an important achievement as related materials often experience a decrease in CO_2 uptake capacity in the presence of water. Two different cycling breakthrough measurements were then carried out to demonstrate the long-term stability and performance of this series: i) a 5-cycle measurement using the same high-humidity conditions as before (CO_2/N_2, $v/v = 15:85$ at 298 K, 1.0 bar, 85 % RH, and a flow rate of 1.0 $mL min^{-1}$); and ii) a 30-cycle measurement using simulated flue gas (80 % N_2, 15 % CO_2, 5 % O_2, 1000 ppm of SO_2, 500 ppm of NO_2, and a flow rate of 1.0 $mL min^{-1}$). For the first high-humidity measurement, after 5 consecutive cycles, there was no loss in CO_2 capture performance, and regeneration between each cycle required minimal energy input (simple He purge at 298 K) (Figure 2h and Section S9 in the Supporting Information). Remarkably, the same findings were true for ZIF-1001 after being exposed to simulated flue gas for 30 consecutive cycles (Figure 2i).

Ethane (C_2H_6) and CO_2 are the main components of tail gas produced during shale gas extraction. Due to the fact that C_2H_6 and CO_2 form a homogeneous binary azeotrope, conventional separation technology based on high temperature and high pressure is inefficient and energy-intensive. ZIFs are well-positioned to be applied toward this process as they have the potential to consistently separate C_2H_6 and CO_2 at normal temperature and pressure.[17] Accordingly, to assess this series' ability to separate C_2H_6 and CO_2, we first measured thermodynamic C_2H_6 adsorption isotherms. The C_2H_6 uptake capacity was estimated from the adsorption isotherms at 298 K, from which ZIF-1001 was demonstrated to have the highest C_2H_6 uptake of 20.6 $cm^3_{STP} g^{-1}$ (Figure 2j). Coverage-dependent isosteric heats of adsorption were calculated via the Clausius–Clapeyron equation by fitting the C_2H_6 adsorption isotherms at 273, 283, and 298 K for each member of the series (Section S7 in the Supporting Information). ZIF-1001 to -1004 displayed similar zero-coverage enthalpies of adsorption (e.g., >30 $kJ mol^{-1}$). Following this, the C_2H_6/CO_2 adsorption selectivity for a C_2H_6/CO_2 binary gas mixture ($v/v = 50:50$) was calculated using IAST by fitting C_2H_6 and C_2H_6 adsorption isotherms at 298 K and 0–100 kPa (Figure 2k and Section S8 in the Supporting Information). From the series, ZIF-1001 exhibited the highest C_2H_6/CO_2 selectivity of 8. To assess the dynamic C_2H_6/CO_2 separation performance of this series, breakthrough experiments were again undertaken, in which ZIF-1001 to -1004 were each subjected to a mixed gas stream at 298 K consisting of 0.5 $mL min^{-1}$ C_2H_6 and 0.5 $mL min^{-1}$ CO_2. Breakthrough curves for ZIF-1001 to -1004 were measured at least two times, with regeneration occurring between each cycle via a He flow (5 $mL min^{-1}$) for 60 min. As shown in Figure 2l, the breakthrough curves demonstrate that all members of the series were capable of effectively and efficiently separating C_2H_6 from CO_2.

Conclusion

It has long been known in both zeolite and ZIF chemistry that making 3-rings is important for accessing new zeolitic structures. Among the hundreds of unique ZIFs reported, it is interesting that there have only been a few discovered (neither designed nor targeted) containing 3-ring motifs. Our findings, therefore, provide a significant addition to the limited library of ZIF design principles. Now, reticular chemists have the requisite tools to explore new ZIF structures that not only have attractive properties (e.g., ultra-high thermal and chemical stability) but also exceptional functions (e.g., practical gas separation under high-humidity and -acidity conditions).

Acknowledgements

This work is supported by the Science and Technology Commission of Shanghai Municipality (Nos. 21XD1402300, 21JC1401700, and 21DZ2260400), the National Natural Science Foundation of China (Nos. 21522105 and 51861145313), the Alliance of International Science Organizations (ANSO-CR-PP-2020-06), and the Jordan Ministry of Higher Education and Scientific Research (BAS/1/6/2020). The authors thank beamlines BL17B and BL14B1 at Shanghai Synchrotron Radiation Facility, the Analytical Instrumentation Center (#SPST-AIC10112914), Prof. Osamu Terasaki, and C*h*EM (#EM02161943) at ShanghaiTech University. K.E.C. acknowledges the Synchrotron-light for Experimental Science and Applications in the Middle East (SESAME; MS Beamline; No. 20190028 and 20210003) for regular beamtime. A.A.A. thanks the financial support from Saudi Aramco (ORCP 2390). A.A.A. and B.A.M. are grateful to KFUPM and KACST-TIC on CCS for financial support (Project No. CCS-15) during the early stages of this work. Finally, we thank Prof. Dr. Omar M. Yaghi, Prof. Dr. Zain H. Yamani, Dr. T. N. Tu and Ms. Rada A. Abaza for their support and helpful discussions throughout the course of this research program.

Conflict of Interest

The authors declare no conflict of interest.

Data Availability Statement

The data that support the findings of this study are available in the supplementary material of this article.

Keywords: Carbon Capture · Gas Separation · Porous Materials · Reticular Chemistry · Zeolitic Imidazolate Frameworks

[1] a) J.-P. Zhang, X.-M. Chen, *Chem. Commun.* **2006**, 1689–1699; b) A. Phan, C. J. Doonan, F. J. Uribe-Romo, C. B. Knobler, M. O'Keeffe, O. M. Yaghi, *Acc. Chem. Res.* **2010**, *43*, 58–67; c) J.-P. Zhang, Y.-B. Zhang, J.-B. Lin, X.-M. Chen, *Chem. Rev.* **2012**, *112*, 1001–1033; d) M. Eddaoudi, D. F. Sava, J. F. Eubank, K. Adil, V. Guillerm, *Chem. Soc. Rev.* **2015**, *44*, 228–249; e) Y.-X. Tan, F. Wang, J. Zhang, *Chem. Soc. Rev.* **2018**, *47*, 2130–2144; f) H. Wang, X. Pei, M. J. Kalmutzki, J. Yang, O. M. Yaghi, *Acc. Chem. Res.* **2022**, *55*, 707–721.

[2] a) Y.-Q. Tian, C.-X. Cai, Y. Ji, X.-Z. You, S.-M. Peng, G.-H. Lee, *Angew. Chem. Int. Ed.* **2002**, *41*, 1384–1386; *Angew. Chem.* **2002**, *114*, 1442–1444; b) X.-C. Huang, J.-P. Zhang, X.-M. Chen, *Chin. Sci. Bull.* **2003**, *48*, 1491–1494; c) X.-C. Huang, Y.-Y. Lin, J.-P. Zhang, X.-M. Chen, *Angew. Chem. Int. Ed.* **2006**, *45*, 1557–1559; *Angew. Chem.* **2006**, *118*, 1587–1589; d) K. S. Park, Z. Ni, A. P. Côté, J. Y. Choi, R. Huang, F. J. Uribe-Romo, H. K. Chae, M. O'Keeffe, O. M. Yaghi, *Proc. Natl. Acad. Sci. USA* **2006**, *103*, 10186–10191.

[3] H. Hayashi, A. P. Côté, H. Furukawa, M. O'Keeffe, O. M. Yaghi, *Nat. Mater.* **2007**, *6*, 501–506.

[4] a) Y.-Q. Tian, Z.-X. Chen, L.-H. Weng, H.-B. Guo, S. Gao, D. Y. Zhao, *Inorg. Chem.* **2004**, *43*, 4631–4635; b) Y.-Q. Tian, Y.-M. Zhao, Z.-X. Chen, G.-N. Zhang, L.-H. Weng, D.-Y. Zhao, *Chem. Eur. J.* **2007**, *13*, 4146–4154; c) Q. Shi, W.-J. Xu, R.-K. Huang, W.-X. Zhang, Y. Li, P. Wang, F.-N. Shi, L. Li, J. Li, J. Dong, *J. Am. Chem. Soc.* **2016**, *138*, 16232–16235.

[5] a) R. Banerjee, A. Phan, B. Wang, C. Knobler, H. Furukawa, M. O'Keeffe, O. M. Yaghi, *Science* **2008**, *319*, 939–943; b) N. T. T. Nguyen, H. Furukawa, F. Gándara, H. T. Nguyen, K. E. Cordova, O. M. Yaghi, *Angew. Chem. Int. Ed.* **2014**, *53*, 10645–10648; *Angew. Chem.* **2014**, *126*, 10821–10824; c) J. Yang, Y.-B. Zhang, Q. Liu, C. A. Trickett, E. Gutiérrez-Puebla, M. Á. Monge, H. Cong, A. Aldossary, H. Deng, O. M. Yaghi, *J. Am. Chem. Soc.* **2017**, *139*, 6448–6455.

[6] a) C. Baerlocher, L. B. McCusker, D. H. Olson, *Atlas of Zeolite Framework Types*, 6th ed., Elsevier, Amsterdam, **2007**; b) C. Baerlocher, L. B. McCusker, *Database of Zeolite Structures* (http://www.iza-structure.org/databases); c) M. D. Foster, M. M. J. Treacy, *Atlas of Prospective Zeolite Structures* (http://www.hypotheticalzeolites.net); d) M. O'Keeffe, M. A. Peskov, S. J. Ramsden, O. M. Yaghi, *Acc. Chem. Res.* **2008**, *41*, 1782–1789; e) O. Delgado-Friedrichs, M. O'Keeffe, O. M. Yaghi, *Reticular Chemistry Structure Resource* (http://rcsr.anu.edu.au/).

[7] a) S. Correll, O. Oeckler, N. Stock, W. Schnick, *Angew. Chem. Int. Ed.* **2003**, *42*, 3549–3552; *Angew. Chem.* **2003**, *115*, 3674–3677; b) A. J. D. Barnes, T. J. Prior, M. G. Francesconi, *Chem. Commun.* **2007**, 4638–4640.

[8] a) G. O. Brunner, W. M. Meier, *Nature* **1989**, *337*, 146–147; b) J. Jiang, J. Yu, A. Corma, *Angew. Chem. Int. Ed.* **2010**, *49*, 3120–3145; *Angew. Chem.* **2010**, *122*, 3186–3212.

[9] a) S. L. Lawton, W. J. Rohrbaugh, *Science* **1990**, *247*, 1319–1322; b) X. Bu, P. Feng, G. D. Stucky, *J. Am. Chem. Soc.* **1998**, *120*, 11204–11205; c) H. Li, M. Eddaoudi, D. A. Richardson, O. M. Yaghi, *J. Am. Chem. Soc.* **1998**, *120*, 8567–8568; d) A. Corma, M. J. Diaz-Cabanas, J. L. Jorda, C. Martinez, M. Moliner, *Nature* **2006**, *443*, 842–845; e) Y. Han, Y. Li, J. Yu, R. Xu, *Angew. Chem. Int. Ed.* **2011**, *50*, 3003–3005; *Angew. Chem.* **2011**, *123*, 3059–3061.

[10] B. Wang, A. P. Côté, H. Furukawa, M. O'Keeffe, O. M. Yaghi, *Nature* **2008**, *453*, 207–211.

[11] T. Wu, X. Bu, R. Liu, Z. Lin, J. Zhang, P. Feng, *Chem. Eur. J.* **2008**, *14*, 7771–7773.

[12] R. Lyndon, W. You, Y. Ma, J. Basca, Y. Gong, E. E. Stangland, K. S. Walton, D. S. Sholl, R. P. Lively, *Chem. Mater.* **2020**, *32*, 3715–3722.

[13] Crystallographic data for ZIF-1001, ZIF-1002, ZIF-1003, and ZIF-1004 were deposited in the Cambridge Crystallographic Data Centre (CCDC). The CCDC deposition numbers are: 2125937 (ZIF-1001), 2125938 (ZIF-1002), 2125943 (ZIF-1003), and 2125939 (ZIF-1004). These data are provided free of charge by the joint Cambridge Crystallographic Data Centre and Fachinformationszentrum Karlsruhe Access Structures service.

[14] a) M. O'Keeffe, M. A. Peskov, S. J. Ramsden, O. M. Yaghi, *Acc. Chem. Res.* **2008**, *41*, 1782–1789; b) V. A. Blatov, O. Delgado-Friedrichs, M. O'Keeffe, D. M. Proserpio, *Acta Crystallogr. Sect. A* **2007**, *63*, 418–425.

[15] a) C. A. Trickett, A. Helal, B. A. Al-Maythalony, Z. H. Yamani, K. E. Cordova, O. M. Yaghi, *Nat. Rev. Mater.* **2017**, *2*, 17045; b) J. M. Kolle, M. Fayaz, A. Sayari, *Chem. Rev.* **2021**, *121*, 7280–7345.

[16] a) P.-Q. Liao, H. Chen, D.-D. Zhou, S.-Y. Liu, C.-T. He, Z. Rui, H. Ji, J.-P. Zhang, X.-M. Chen, *Energy Environ. Sci.* **2015**, *8*, 1011–1016; b) P. G. Boyd, A. Chidambaram, E. García-Díez, C. P. Ireland, T. D. Daff, R. Bounds, A. Gładysiak, P. Schouwink, S. M. Moosavi, M. M. Maroto-Valer, J. A. Reimer,

J. A. R. Navarro, T. K. Woo, S. Garcia, K. C. Stylianou, B. Smit, *Nature* **2019**, *576*, 253–256; c) Z.-S. Wang, M. Li, Y.-L. Peng, Z. Zhang, W. Chen, X.-C. Huang, *Angew. Chem. Int. Ed.* **2019**, *58*, 16071–16076; *Angew. Chem.* **2019**, *131*, 16217–16222; d) Z. Shi, Y. Tao, J. Wu, C. Zhang, H. He, L. Long, Y. Lee, T. Li, Y.-B. Zhang, *J. Am. Chem. Soc.* **2020**, *142*, 2750–2754.

[17] a) S. Kelman, H. Lin, E. S. Sanders, B. D. Freeman, *J. Membr. Sci.* **2007**, *305*, 57–68; b) M. Korpyś, J. Wójcik, P. Synowiec, *Chemik* **2015**, *68*, 211–215; c) J. Duan, M. Higuchi, M. L. Foo, S. Horike, K. P. Rao, S. Kitagawa, *Inorg. Chem.* **2013**, *52*, 8244–8249.

Manuscript received: May 20, 2022
Accepted manuscript online: June 29, 2022
Version of record online: ■■, ■■

Research Articles

Zeolitic Imidazolate Frameworks

X. Zha, X. Li, A. A. Al-Omari, S. Liu, C.-C. Liang, A.'a Al-Ghourani, M. Abdellatief, J. Yang, H. L. Nguyen, B. Al-Maythalony,* Z. Shi,* K. E. Cordova,* Y.-B. Zhang*

Zeolite NPO-Type Azolate Frameworks

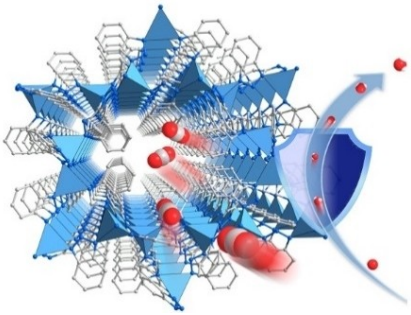

A new design principle for obtaining zeolitic imidazolate frameworks (ZIFs) with an underlying NPO built from three-membered rings (3-rings) is reported. Among the hundreds of unique ZIFs known, only a few have been discovered that are partially constructed from 3-ring motifs. These findings provide a significant addition to the limited library of ZIF design principles to access attractive structural features for realizing practical function.